Supplementary Information

Densely Packed High-Entropy Spinel Nanoparticles Derived from Concentration-Driven MOF Gel for Lithium-Ion Hybrid Capacitors

Yidong Zhang,[a] Hui Cao,[a] Jiale, Liu,[a] Jianfei Ding,[a] Qirui Guo[b], Shixin Sun[b], Yuan Wang*[b]

a School of Chemistry and Chemical Engineering, Yancheng Institute of Technology, Yancheng, 224051, PR China

b School of Chemistry and Environmental Engineering, Yancheng Teachers University, Yancheng, 224002, PR China

*Corresponding author:

* Yuan Wang **E-mail**: wangy03@yctu.edu.cn

Table S1 Performance comparison among reported high-entropy materials synthesized by different methods.

High-entropy Materials	Synthesis Methods	Tunability of stacking structure	Surface area	Reference
$(Cr_{0.2}Mn_{0.2}Fe_{0.2}Co_{0.2}Ni_{0.2})_3O_4$	**MOF-gel Method**	**Yes**	**32.7-6.3 $m^2 g^{-1}$**	**This work**
$(MnFeCoNiCu)_3O_4$	Thermal Plasma Reaction	No	15.6 $m^2 g^{-1}$	[1] (**2024**)
CoCrNiFeMn HEA	Induction Melting Method	No	25 $m^2 g^{-1}$	[2] (**2023**)
$(Co_{0.2}Cr_{0.2}Fe_{0.2}Mn_{0.2}Ni_{0.2})_3O_4$	Polyacrylamide gel Method	No	25.17 $m^2 g^{-1}$	[3] (**2023**)
$(W_{28}Ni_{24}Co_{24}Mo_{17}Ru_7)PO_x/C$	MOF-annealing Method	No	5.8 $m^2 g^{-1}$	[4] (**2022**)
$(LaY)(Zr_{0.5}Ti_{0.5}Ce_{0.5}Hf_{0.5})O_7$	Sol-gel Method	No	4.05 $m^2 g^{-1}$	[5] (**2022**)
$(Mg_{0.2}Ti_{0.2}Zn_{0.2}Cu_{0.2}Fe_{0.2})_3O_4$	High-energy ball-milling	No	12.31 $m^2 g^{-1}$	[6] (**2020**)
AlCoCrFeNi HEA	Arc Melting Method	No	27.8 $m^2 g^{-1}$	[7] (**2019**)

Note: References used in the table are all listed at the end of this document.

Table S2 Supercapacitive performance comparison among different high-entropy material-based electrodes.

Electrode Material	Synthesis method	Specific capacitance	Electrolyte	References
$(Cr_{0.2}Mn_{0.2}Fe_{0.2}Co_{0.2}Ni_{0.2})_3O_4$	**MOF-gel method**	**636.4 F g^{-1} at 1 A g^{-1}**	**1 M LiOH**	**This work**
$(Mg_{0.21}Cr_{0.21}Mn_{0.21}Fe_{0.21}Cu_{0.16})_3O_4$	Sol-gel method	241 F g^{-1} at 1 A g^{-1}	1 M KOH	[8] **2025**
$(FeCoNiCrMn)_3O_4$	Solid state sintering	391.1 F g^{-1} at 0.5 A g^{-1}	1 M $(NH_4)_2SO_4$	[9] **2025**
$(CrMnFeCoNiLi)_3O_4$	Sol-gel method	550.35 F g^{-1} at 0.5 A g^{-1}	1 M KOH	[10] **2025**
$(MnFeCoNiCu)_3O_4$	Thermal plasma reaction	431 F g^{-1} at 0.5 A g^{-1}	1 M KOH	[11] **2024**
$(FeCoNiCuMn)_3O_4$	Liquid state induction melting	313 F g^{-1} at 5 mV s^{-1}	3 M KOH	[12] **2024**
$(FeCoCrMnNi)_3O_4$	Sol-gel method	204 F g^{-1} at 0.5 A g^{-1}	1 M KOH	[13] **2024**
$(FeCoNiCuZn)_3O_4$	Induction melting	245.7 F g^{-1} at 1.5 A g^{-1}	3 M KOH	[14] **2024**
$(Mn, Ni, Mo, Co, Fe)_3O_4$	Thermal plasma	215 F g^{-1} at 2 A g^{-1}	1 M KOH	[15] **2024**
$(Co_{0.2}Cr_{0.2}Fe_{0.2}Mn_{0.2}Ni_{0.2})_3O_4$	Polyacrylamide gel method	384 F g^{-1} at 1 A g^{-1}	6 M KOH	[16] **2023**
$(FeCoCrMnNi)_3O_4$	Sol-gel method	332.2 F g^{-1} at 0.3 A g^{-1}	1 M KOH	[17] **2023**
$(FeCoCrMnMg)_3O_4$	Solid-state reaction	193.7 F g^{-1} at 1 A g^{-1}	1 M KOH	[18] **2021**
$(CrMnFeCoNi)_3O_4$	Co-precipitation	239 F g^{-1} at 0.5 A g^{-1}	2 M KOH	[19] **2021**

Note: References used in the table are all listed at the end of this ESI document.

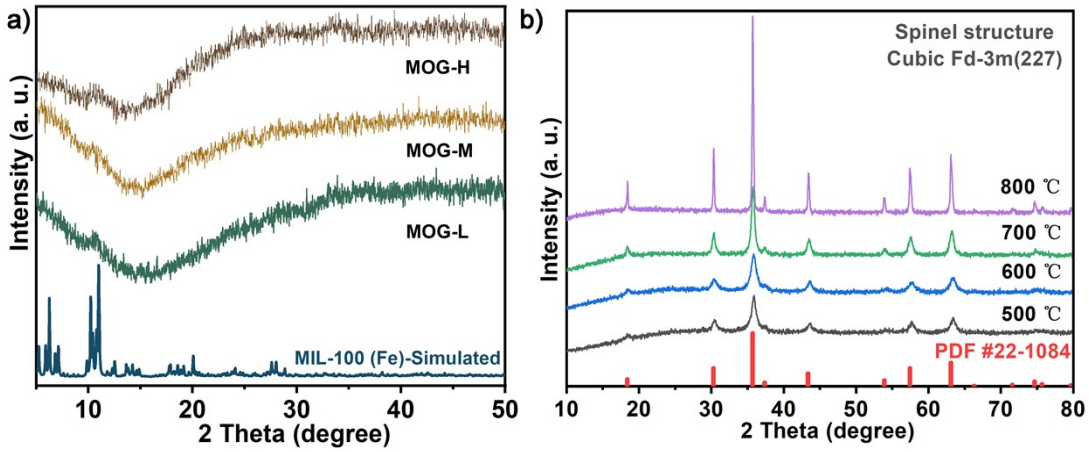

Fig. S1 (a) XRD pattern of MOF gel precursor; (b) XRD patterns of the products obtained after calcining MOG-L at various temperatures ranging from 500 to 800 °C.

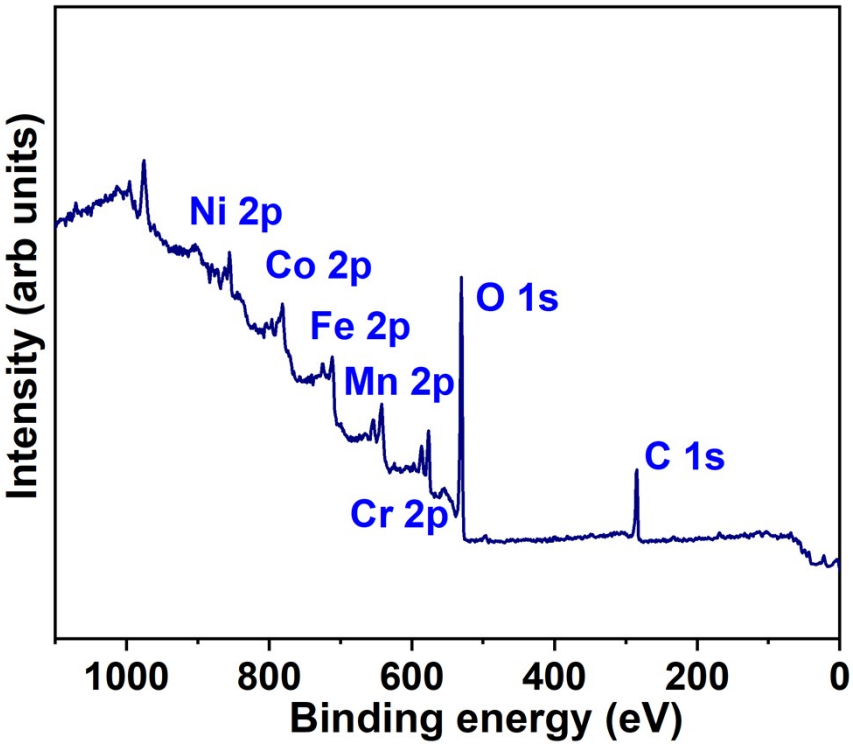

Fig. S2 XPS survey spectrum of $(Cr_{0.2}Mn_{0.2}Fe_{0.2}Co_{0.2}Ni_{0.2})_3O_4$.

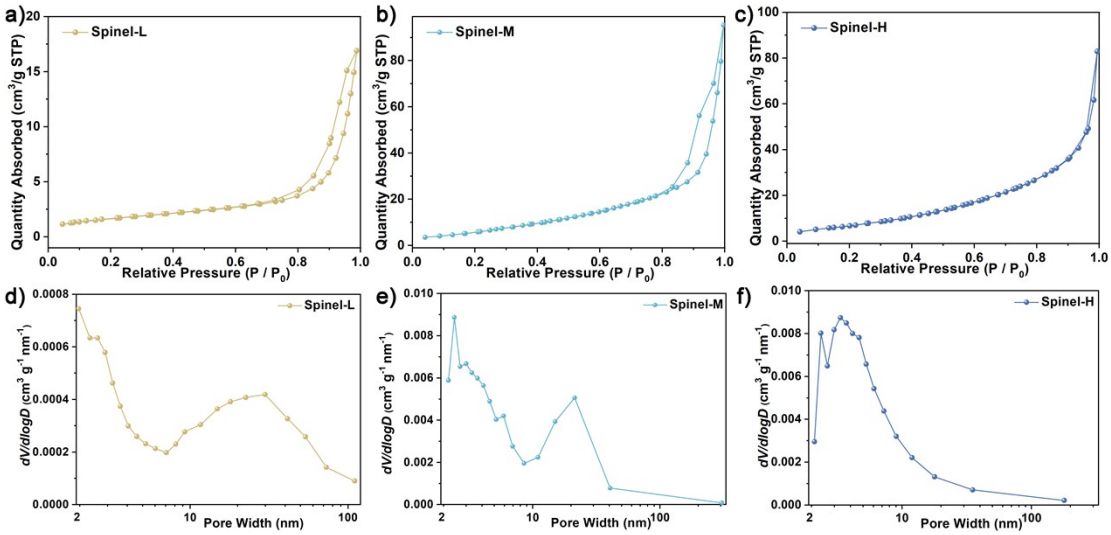

Fig. S3 Pore structure characterization of HEO nanoparticles synthesized with different MOF gel precursor: (a), (b), (c) N_2 adsorption/desorption isotherms of Spinel-L, Spinel-M, Spinel-H; (d), (e), (f) pore size distribution of Spinel-L, Spinel-M, Spinel-H.

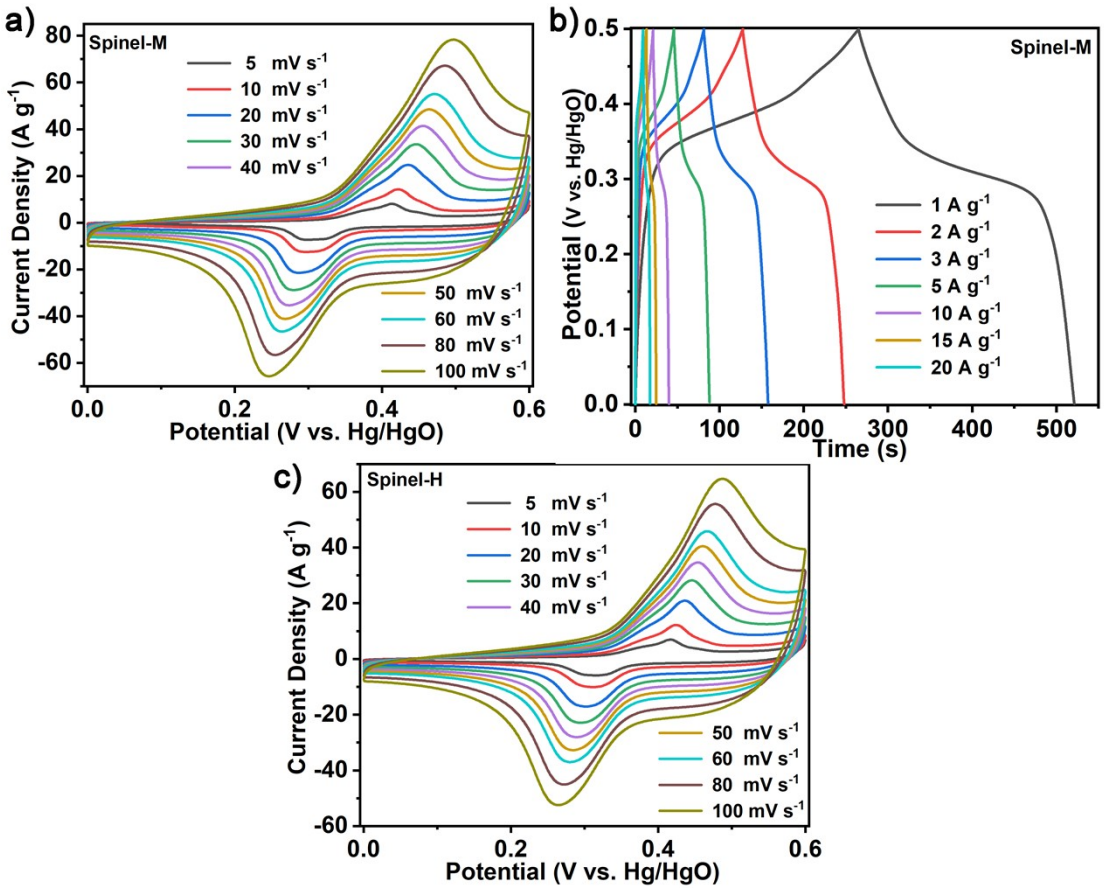

Fig. S4 Electrochemical performance of HEO nanoparticles synthesized with different MOF gel precursor: (a) CV curves of Spinel-M at different scan rates; (b) GCD curves of Spinel-M at different current densities; (c) CV curves of Spinel-H at different scan rates.

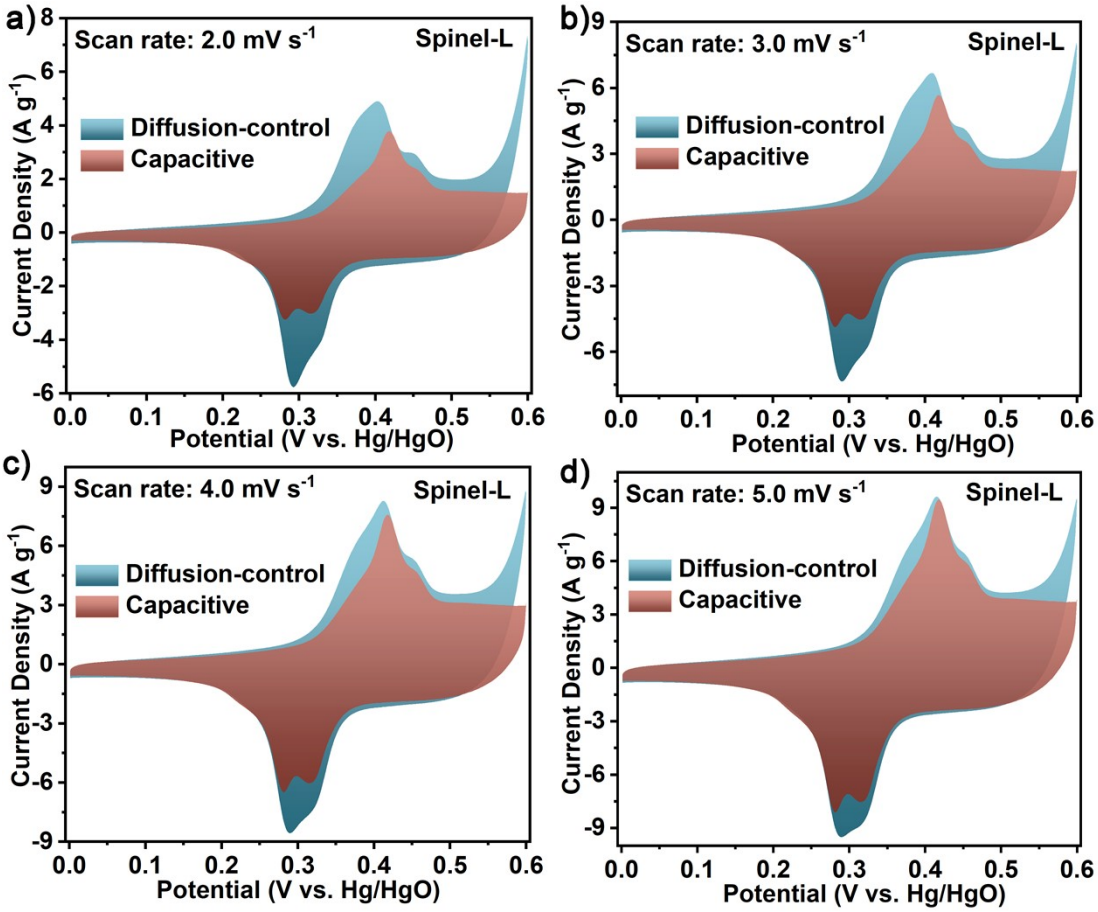

Fig. S5 Electrode kinetics analysis of Spinel-L, the corresponding shadow area of capacitive/diffusion contribution at different scan rates: (a) 2.0 mV s^{-1}; (b) 3.0 mV s^{-1}; (c) 4.0 mV s^{-1}; (d) 5.0 mV s^{-1}.

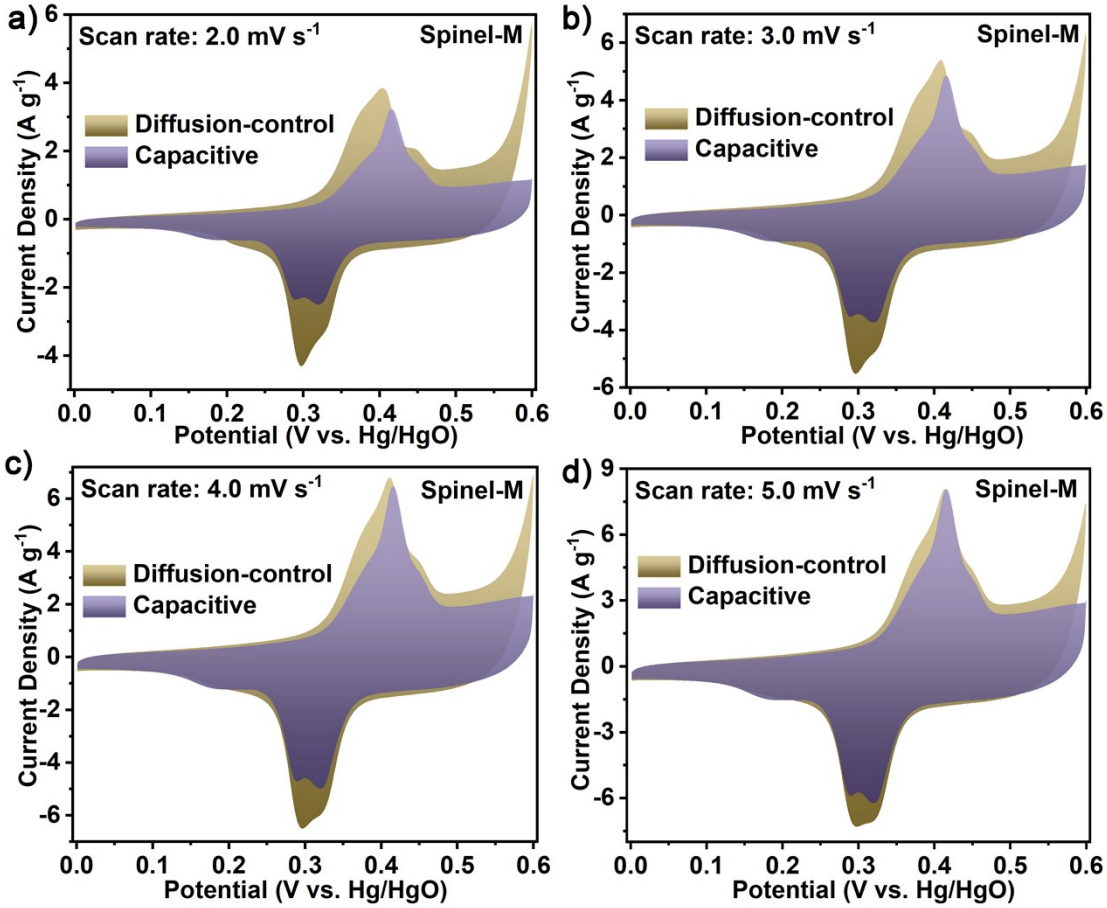

Fig. S6 Electrode kinetics analysis of Spinel-M, the corresponding shadow area of capacitive/diffusion contribution at different scan rates: (a) 2.0 mV s^{-1}; (b) 3.0 mV s^{-1}; (c) 4.0 mV s^{-1}; (d) 5.0 mV s^{-1}.

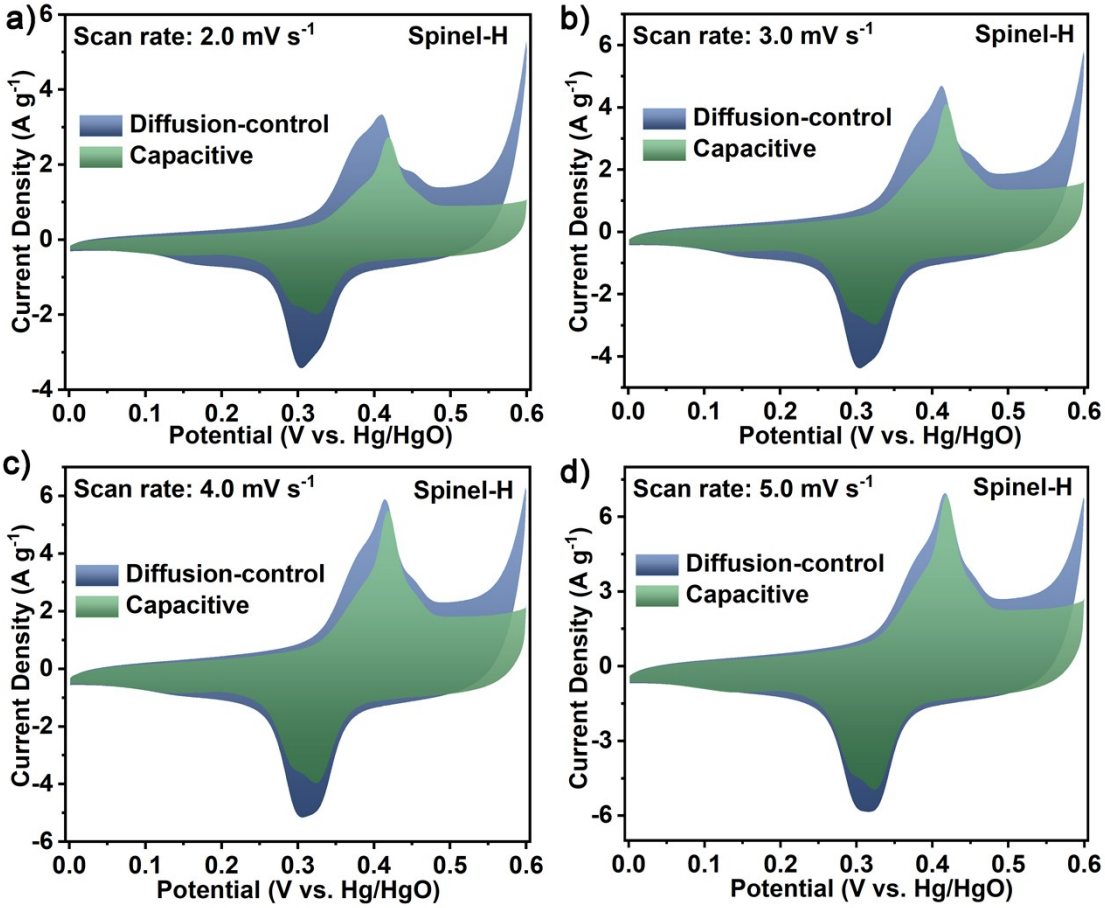

Fig. S7 Electrode kinetics analysis of Spinel-H, the corresponding shadow area of capacitive/diffusion contribution at different scan rates: (a) 2.0 mV s^{-1}; (b) 3.0 mV s^{-1}; (c) 4.0 mV s^{-1}; (d) 5.0 mV s^{-1}.

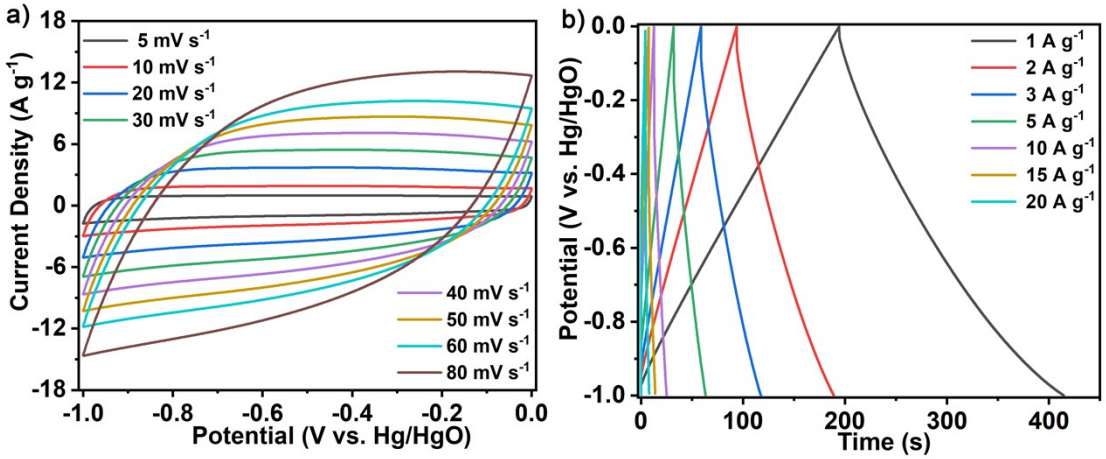

Fig. S8 Electrochemical performance of active carbon in a three-electrode system: (a) CV curves at different scan rates; (b) GCD curves at different current densities.

References

[1] A. Pasupathi, Y. Subramaniam, A Novel Strategy for Rapid Synthesis of Nanostructured High-Entropy Metal Oxides through Thermal Plasma for Supercapacitor Applications, *Energy Fuels*, **2024**, *38*, 5534-5544.

[2] G.C. Mohanty, C.C. Gowda, P. Gakhad, M. Sanjay, S. Sarkar, K. Biswas, A. Singh, C.S. Tiwary, High energy density liquid state asymmetric supercapacitor devices using Co-Cr-Ni-Fe-Mn high entropy alloy, *Mater. Adv.*, **2023**, *4*, 3839-3852.

[3] L. Li, P. Ji, C. Geng, Y. Li, L. Meng, B. Zhou, J. Liang, J. Peng, X. Su, Facile synthesis of high-entropy $(Co_{0.2}Cr_{0.2}Fe_{0.2}Mn_{0.2}Ni_{0.2})_3O_4$ nanopowders and their electrochemical properties as supercapacitor electrode, *J. Energy Storage*, **2023**, *73*, 109182.

[4] Z. Wang, X. Zhang, X. Wu, Y. Pan, H. Li, Y. Han, G. Xu, J. Chi, J. Lai, L. Wang, High-entropy phosphate/C hybrid nanosheets for efficient acidic hydrogen evolution reaction, *Chem. Eng. J.*, **2022**, *437*, 135375.

[5] P. Tang, Y. Cao, l. Hao, M. Lu, W. Qiu, The preparation of high-performance aqueous supercapacitor with high-entropy pyrochlore-type electrode and super-concentrated electrolyte, *Ceram. Int.*, **2022**, *48*, 2660-2669.

[6] H. Chen, N. Qiu, B. Wu, Z. Yang, S. Sun, Y. Wang, A new spinel high-entropy oxide $(Mg_{0.2}Ti_{0.2}Zn_{0.2}Cu_{0.2}Fe_{0.2})_3O_4$ with fast reaction kinetics and excellent stability as an anode material for lithium ion batteries, *RSC Adv.*, **2020**, *10*, 9736-9744.

[7] K. Kong, J. Hyun, Y. Kim, W. Kim, D. Kim, Nanoporous structure synthesized by selective phase dissolution of AlCoCrFeNi high entropy alloy and its electrochemical properties as supercapacitor electrode, *J. Power Sources*, **2019**, *437*, 226927.

[8] K. Chillal, A. Halder, S.K. Jha, R. Patel, J. Valand, Electrochemical investigation of synthesized $(Mg_{0.21}Cr_{0.21}Mn_{0.21}Fe_{0.21}Cu_{0.16})_3O_4$ high entropy oxide for

supercapacitor electrode material, *Ceram. Int.*, **2025**, *51*, 3890-3898.

[9] F. Long, L. Zhang, Y. Gao, Enabling a High-Entropy Effect Paradigm for Efficient Zn^{2+}/NH^{4+} Energy Storage, *Adv. Energy Mater.*, **2025**, *15*, e04021.

[10] B. Chen, W.-B. Zhang, J. Feng, J.-X. Li, F. Yang, K. Yang, X.-Y. Liu, X.-J. Ma, Elemental Modulation Inducing Defect Engineering to Enhance Electrochemical Capacitance and Rectification Performance of High-Entropy Oxides, *Inorg. Chem.*, **2025**, *64*, 8923-8936.

[11] A. Pasupathi, Y. Subramaniam, A Novel Strategy for Rapid Synthesis of Nanostructured High-Entropy Metal Oxides through Thermal Plasma for Supercapacitor Applications, *Energy & Fuels*, **2024**, *38*, 5534-5544.

[12] G. Chandra Mohanty, S. Das, A. Verma, Synthesis of $(FeCoNiCuMn)_3O_4$ spinel-high entropy oxide and green carbon from agricultural waste for supercapacitor application, *RSC Adv.*, **2024**, *14*, 33830-33842.

[13] Y. Yin, W.-B. Zhang, B. Chen, J. Feng, J.-L. Yang, Z.-Q. Yang, J.-J. Li, X.-J. Ma, Porous powder synthesis of $(FeCoCrMnNi)_3O_4$ high entropy ceramic and its supercapacitor applications, *Ceram. Int.*, **2024**, *50*, 10292-10304.

[14] G.C. Mohanty, S. Das, A. Verma, Fabrication of aqueous asymmetric supercapacitor device by using spinel type $(FeCoNiCuZn)_3O_4$ high entropy oxide and green carbon derived from plastic wastes, *Ceram. Int.*, **2024**, *50*, 48938-48947.

[15] A. Pasupathi, M. Perumal, E. Narayanamoorthi, B. Palanisamy, Y. Subramaniam, Electrochemical charge storage performance of $(Mn, Ni, Mo, Co, Fe)_3O_4$ high entropy oxide nanoparticles produced via thermal plasma route, *Ceram. Int.*, **2024**, *50*, 26740-26749.

[16] L. Li, P. Ji, C. Geng, Y. Li, L. Meng, B. Zhou, J. Liang, J. Peng, X. Su, Facile synthesis of high-entropy $(Co_{0.2}Cr_{0.2}Fe_{0.2}Mn_{0.2}Ni_{0.2})_3O_4$ nanopowders and their

electrochemical properties as supercapacitor electrode, *J. Energy Storage*, **2023**, *73*, 109182.

[17] Y. Yin, W.-B. Zhang, X.-L. Zhang, M.M. Theint, J.-L. Yang, Z.-Q. Yang, J.-J. Li, S. Liang, X.-J. Ma, Low-dimensional high entropy oxide $(FeCoCrMnNi)_3O_4$ for supercapacitor applications, *Dalton Trans.*, **2023**, *52*, 9005-9016.

[18] Y. Wang, Y. Ai, S. Yang, B. Liang, Z. Zheng, S. Ouyang, W. He, W. Chen, C. Liu, J. Zhang, Z. Liu, Facile Synthesis and Supercapacitor Performance of M_3O_4(M=FeCoCrMnMg) High Entropy Oxide Powders, *J. Inorg. Mater.*, **2020**, *36*, 425-430.

[19] B. Talluri, M.L. Aparna, N. Sreenivasulu, S.S. Bhattacharya, T. Thomas, High entropy spinel metal oxide $(CoCrFeMnNi)_3O_4$ nanoparticles as a high-performance supercapacitor electrode material, *J. Energy Storage*, **2021**, *42*, 103004.